

# Cell-to-cell coupling in engineered pairs of rat ventricular cardiomyocytes: relation between Cx43 immunofluorescence and intercellular electrical conductance

Megan L. McCain, Thomas Desplantez, Nicholas A. Geisse, Barbara Rothen-Rutishauser, Helene Oberer, Kevin Kit Parker and Andre G. Kleber

*Am J Physiol Heart Circ Physiol* 302:H443-H450, 2012. First published 11 November 2011;  
doi:10.1152/ajpheart.01218.2010

## You might find this additional info useful...

---

Supplemental material for this article can be found at:

<http://ajpheart.physiology.org/content/suppl/2011/11/22/ajpheart.01218.2010.DC1.html>

This article cites 35 articles, 19 of which can be accessed free at:

<http://ajpheart.physiology.org/content/302/2/H443.full.html#ref-list-1>

Updated information and services including high resolution figures, can be found at:

<http://ajpheart.physiology.org/content/302/2/H443.full.html>

Additional material and information about *AJP - Heart and Circulatory Physiology* can be found at:

<http://www.the-aps.org/publications/ajpheart>

---

This information is current as of January 6, 2012.

# Cell-to-cell coupling in engineered pairs of rat ventricular cardiomyocytes: relation between Cx43 immunofluorescence and intercellular electrical conductance

Megan L. McCain,<sup>3</sup> Thomas Desplantez,<sup>1</sup> Nicholas A. Geisse,<sup>3</sup> Barbara Rothen-Rutishauser,<sup>2</sup> Helene Oberer,<sup>1</sup> Kevin Kit Parker,<sup>3</sup> and Andre G. Kleber<sup>1</sup>

Departments of <sup>1</sup>Physiology and <sup>2</sup>Anatomy, University of Bern, Bern, Switzerland; and <sup>3</sup>Disease Biophysics Group, Wyss Institute for Biologically-Inspired Engineering, Harvard School of Engineering and Applied Sciences, Cambridge, Massachusetts

Submitted 6 December 2010; accepted in final form 3 November 2011

**McCain ML, Desplantez T, Geisse NA, Rothen-Rutishauser B, Oberer H, Parker KK, Kleber AG.** Cell-to-cell coupling in engineered pairs of rat ventricular cardiomyocytes: relation between Cx43 immunofluorescence and intercellular electrical conductance. *Am J Physiol Heart Circ Physiol* 302: H443–H450, 2012. First published November 11, 2011; doi:10.1152/ajpheart.01218.2010.—Gap junctions are composed of connexin (Cx) proteins, which mediate intercellular communication. Cx43 is the dominant Cx in ventricular myocardium, and Cx45 is present in trace amounts. Cx43 immunosignal has been associated with cell-to-cell coupling and electrical propagation, but no studies have directly correlated Cx43 immunosignal to electrical cell-to-cell conductance,  $g_j$ , in ventricular cardiomyocyte pairs. To assess the correlation between Cx43 immunosignal and  $g_j$ , we developed a method to determine both parameters from the same cell pair. Neonatal rat ventricular cardiomyocytes were seeded on micropatterned islands of fibronectin. This allowed formation of cell pairs with reproducible shapes and facilitated tracking of cell pair locations. Moreover, cell spreading was limited by the fibronectin pattern, which allowed us to increase cell height by reducing the surface area of the pattern. Whole cell dual voltage clamp was used to record  $g_j$  of cell pairs after 3–5 days in culture. Fixation of cell pairs before removal of patch electrodes enabled preservation of cell morphology and offline identification of patched pairs. Subsequently, pairs were immunostained, and the volume of junctional Cx43 was quantified using confocal microscopy, image deconvolution, and three-dimensional reconstruction. Our results show a linear correlation between  $g_j$  and Cx43 immunosignal within a range of 8–50 nS.

electrical cell-to-cell coupling; cell engineering; microcontact printing; dual voltage clamp

CONNEXINS (CX) ARE PROTEINS that assure cell-to-cell transfer of ions and small regulatory molecules and are important determinants of cardiac electrical function. Cardiac tissue expresses three major Cx, Cx43, Cx40, and Cx45, which show specific distributions in various cardiac regions (9, 19, 32). In ventricular myocardium, Cx43 is the dominant protein, and Cx45 is present in small amounts. In certain species, Cx45 modifies average gap junction channel conductance (3). Cx43 and Cx45 are remodeled in pathophysiological states; in the case of cardiac failure, downregulation of Cx43 and upregulation of Cx45 are observed (1, 12, 35).

The amount of Cx expressed by cardiomyocytes is known to play an important role in cardiac electrical function. Measurement of Cx by Western blot provides information about total

cellular Cx, but may not necessarily be related to the Cx contributing to gap junction channels (4). Comparison of Cx43 immunosignals in gap junctions with gap junction plaque dimensions assessed by electron microscopy suggests that Cx43 immunosignal is a reliable measure of the gap junction area in which Cx43 is distributed (24). Relating altered levels of Cx43 in gap junctions, induced either by remodeling or genetic ablation, to electrical propagation suggests that there is a quantitative relationship between the Cx43 immunosignal measured over an area comprising >100 cells and propagation velocity (4, 8, 27, 28). However, experimental and theoretical work indicate that propagation velocity is not linearly related to cell-to-cell coupling and is relatively insensitive to moderate changes of normal cell-to-cell coupling (20).

The goal of the present study was to directly compare the Cx43 immunosignal in a pair of cultured ventricular cardiomyocytes to the electrical properties of its cell-to-cell junction. To this aim, we developed a method for generating cell pairs of controlled dimensions using microcontact printing. This also enabled us to consistently generate cell pairs with specific dimensions, allowing us to understand how cell shape can modify gap junction size. We used a method for preserving and immunostaining cell pairs after patch clamp by applying fixative while the patch clamp pipettes were still attached to the cell membranes. This allowed us to obtain electrical measurements and Cx43 immunostaining data from the same cell pair. Our results suggest a direct correlation between Cx43 immunosignal and electrical intercellular conductance,  $g_j$ , within a range of  $g_j$  values from 8 to 50 nS.

## MATERIAL AND METHODS

**Photolithography, micropatterning, and cell culture.** A photolithographic mask was designed in AutoCAD (Autodesk, San Rafael, CA) to produce cell pairs with control of cell shape. The mask design consisted of arrays of two rectangles (dimensions:  $40 \times 12 \mu\text{m}^2$ ,  $60 \times 12 \mu\text{m}^2$ , or  $80 \times 12 \mu\text{m}^2$ ) paired along their short axis with a 2- $\mu\text{m}$  separation (Fig. 1, A and B). A given group of 8–12 pairs was outlined with a 100- $\mu\text{m}$ -thick rectangular cell adhesion region serving as a conditional cell layer and labeled with a number and letter (Fig. 1A). This label facilitated offline identification of cell pairs.

Standard soft lithography techniques were used to create polydimethylsiloxane (PDMS) (Dow Corning, Midland, MI) stamps for microcontact printing, as previously reported (5, 15). Briefly, silicon wafers (Wafer World, West Palm Beach, FL) were spin-coated with SU-8 2002 photoresist (MicroChem, Newton, MA) to form a 2- $\mu\text{m}$  layer on the surface. The wafer was aligned under the photolithographic mask described above using a mask aligner (ABM, Scotts Valley, CA) and then exposed to UV light and submersed in propylene glycol methyl ether acetate to dissolve the regions not blocked by

Address for reprint requests and other correspondence: A. G. Kléber, Dept. of Pathology, Beth Israel Deaconess Medical Center, Harvard Medical School, DANA 752, 330 Brookline Ave., Boston, MA 02215 (e-mail: akleber@bidmc.harvard.edu).

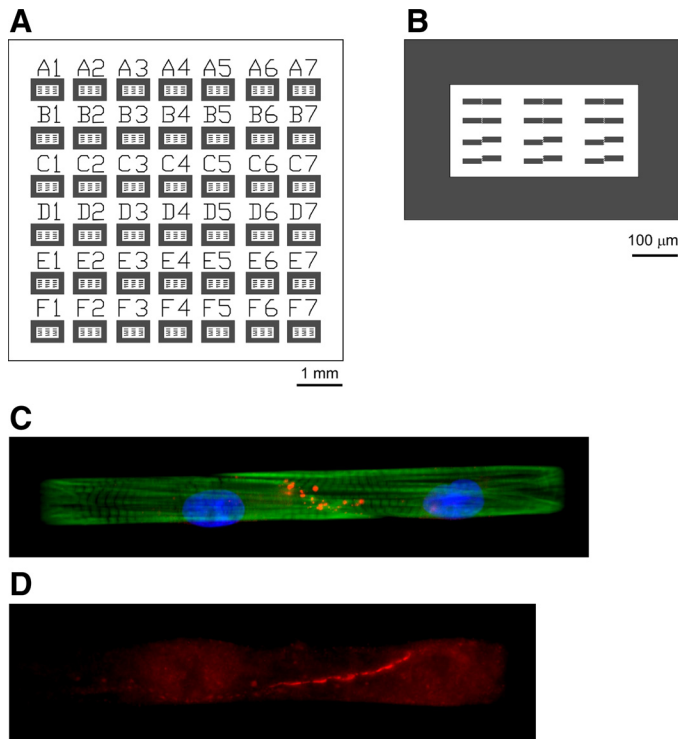


Fig. 1. Fabrication of engineered cell pairs. *A*: the photolithographic mask consists of an array of blocks, with each block containing patterns for 8–12 cell pairs. Blocks are labeled with letters and numbers to serve for offline identification of cell pairs. *B*: each block contains cells growing on a rectangular frame. Within each frame, 8–12 cell pairs are patterned with a staggered or nonstaggered interface. *C*: cell pair in a nonstaggered arrangement showing Cx43 immunofluorescence (red), nuclei [4,6-diamidino-2-phenylindole (DAPI), blue], and actin (phalloidin, green). *D*: cell pair in a nonstaggered arrangement showing connexin (Cx) 45 fluorescence (red).

the mask. PDMS was poured over the wafer and allowed to polymerize, at which point it was peeled off the wafer and cut into smaller sizes to be used as stamps. PDMS stamps (26) were coated with 25  $\mu\text{g}/\text{ml}$  fibronectin (Sigma-Aldrich, St. Louis, MO), and glass coverslips spin-coated with PDMS were treated in a UV-ozone cleaner (Jelight, Irvine, CA) before stamping. The fibronectin-coated stamps were placed on the coverslips to transfer fibronectin in the desired pattern, which were subsequently immersed in 1% Pluronic F108 (BASF, Ludwigshafen, Germany) to block cell adhesion to unpatterned areas.

Ventricular tissue from 2-day old Sprague-Dawley rat hearts was minced, and a cell suspension was obtained by enzymatic digestion (22). The cell suspension was preplated to eliminate fibroblasts and subsequently seeded on the PDMS-coated coverslips at a concentration of 250,000 cells/coverslip. All animal procedures were approved by the State Veterinary Department and the Swiss National Science Foundation.

**Dual-voltage clamp.** The methods utilized to assess the junctional conductance,  $g_j$ , and conductance of a single gap junction channel,  $\gamma_j$ , in cell pair preparations, superfusion solutions, and pipette filling solutions have been described previously in detail (10). Electrophysiological measurements were performed using an EPC 10 dual-patch clamp amplifier (HEKA). Patch electrodes were pulled using a DMZ puller (Zeitz) and filled with a solution containing the following (in  $\text{mmol}/\text{l}$ ): 120  $\text{K}^+$ , 10  $\text{Na}^+$ , 1  $\text{Ca}^{2+}$ , 120 aspartate, 2  $\text{Cl}^-$ , 5 HEPES, 10 EGTA, and 3  $\text{Mg-ATP}$ , at a  $\text{pH} = 7.3$ . Pipette tip resistances ranged from 2 to 4.8  $\text{M}\Omega$  ( $3.2 \pm 0.27 \text{ M}\Omega$ ). After establishment of electrode seals, electrode access resistances were in a close range ( $9.3 \pm 0.35 \text{ M}\Omega$ ), as previously reported (34). The membrane resistance of the patterned neonatal ventricular myocytes amounted to  $2.76 \pm 0.35 \text{ G}\Omega$

(34). Engineered pairs (3–5 days in culture) were selected to measure the transjunctional current ( $I_j$ ) and to determine  $g_j$  ( $g_j = I_j/V_j$ ), where  $V_j$  is junctional voltage, using dual-voltage clamp (DVC) and the whole cell recording mode at room temperature. In the majority of cultures, blebbistatin (10  $\mu\text{M}$ ) was added to eliminate contraction (14). Initially, both cell membrane potentials ( $V_m$ ) were clamped at  $V_{m1} = V_{m2} = 0 \text{ mV}$  to prevent the interference of any nonjunctional membrane current. Thereafter, a 10-mV voltage pulse was administered to cell 1, and  $I_j$  was measured from cell 2. Cell pairs treated with heptanol (2.5  $\text{mmol}/\text{l}$ ) were used to determine  $\gamma_j$  with voltage pulses of different amplitude and of different polarity (29). As expected, the absence of a significant difference between current 1 ( $I_1$ ) and current 2 ( $I_2$ ) ( $I_1 = -I_2$ ) indicated that the measurement of  $g_j$  was not affected by any shunt current through the membrane resistances of the two cells (31). In such a case, the calculation of the “true”  $g_j$  can be made using a simplified electrical circuit consisting of the gap junction resistance in series with the two access resistances of the patch electrodes. Therefore, to obtain the true value of  $g_j$ , the measured value was corrected using the value of the mean access resistance of 9.3  $\text{M}\Omega$ . Since each measurement of  $g_j$  and the corresponding three-dimensional (3D) analysis of the Cx43 immunosignal in the same cell pair implicated immediate fixation of the preparation with the patch electrodes attached, only one measurement was obtained per cell culture.

To determine the  $\gamma_j$  with voltage pulses of different amplitude and of different polarity (29), cell pairs treated with heptanol (2.5  $\text{mmol}/\text{l}$ ) were used. Measurements of  $\gamma_j$  were obtained in a total of 7 different cell cultures from 32 different cell pairs. In these measurements, single-channel events ( $n = 745$ ) lasting  $> 10 \text{ ms}$  were identified from current traces showing maximally three distinct levels (13). In nine cell pairs, only one channel event was observed during the application of both a negative and a positive  $V_j$ . The abrupt change in junctional channel current amplitude, and accordingly in  $\gamma_j$ , was used for detection of asymmetrical gating, suggesting the presence of heteromeric Cx43/Cx45 connexons.

Data acquisition was done in “Pulse”; data analysis and curve fitting were done in “PulseFit” (HEKA Electronic, Lambrecht, Germany) and “SigmaPlot” (Systat, San Jose, CA).

**Immunostaining, confocal microscopy, and image deconvolution.** Immediately after electrical recordings were completed, the Tyrode bath solution was replaced with 4% paraformaldehyde (5 min) for cell fixation, while the electrodes remained attached to the cells. The bath was then rinsed with HBSS (Invitrogen, Carlsbad, CA), and the pipettes were slowly retracted. This preserved the morphology of the patched cells, which is usually destroyed on pipette retraction, if the cells are alive. The location of the patched cell pair was noted using the indexing system mentioned above (Fig. 1A).

Fixed cells were incubated in blocking buffer (HBSS with 10% bovine serum albumin, 0.15% Triton X-100, 3% normal goat serum) for 30 min at room temperature. Certain coverslips were stained with 4,6-diamidino-2-phenylindole (D1306, Invitrogen, Carlsbad, CA) and Alexa Fluor 488 Phalloidin (A12379, Invitrogen) for visualization purposes (Fig. 1C). Anti-Cx43 (MAB 3068, Chemicon, Billerica, MA) primary antibodies were diluted 1:200 in blocking buffer and applied in a humid chamber overnight at  $4^\circ\text{C}$ . Secondary antibodies (T-2762, Tetramethylrhodamine, Invitrogen) were diluted 1:200 in blocking buffer and applied for 2 h at room temperature. In some experiments, Cx45 was visualized with anti-Cx45 antibody (18) (kindly provided by Dr. T. Steinberg and Dr. K. Yamada, St. Louis, MO). The Cx45 immunosignal was faint relative to the Cx43 signal. This excluded analysis using image deconvolution and 3D reconstruction of the Cx45 immunosignal (Fig. 1D). Coverslips were mounted on glass slides using ProFade Gold Antifade Reagent (Invitrogen) and sealed with clear nail polish.

Immunostained cells were imaged with a Zeiss LSM 510 confocal microscope using a Plan-Apochromat  $\times 100$  numerical aperture 1.4 oil differential interference contrast objective to collect both Cx43 immunofluorescence and bright-field images. High-resolution image

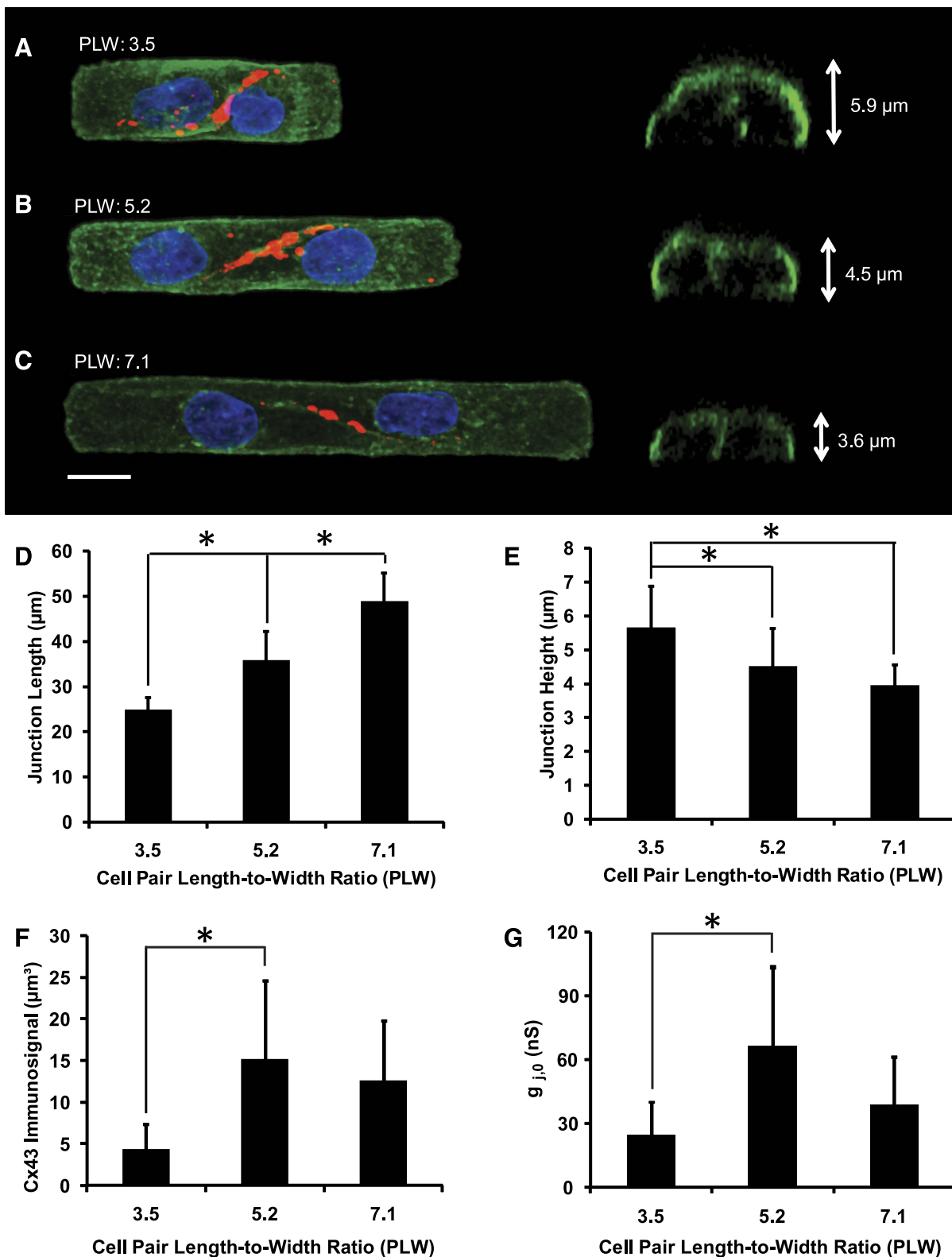


Fig. 2. *A–C*: three-dimensional (3D) morphology of cell pairs. *Left*: maximum *z*-projections of wheat germ agglutinin (WGA) stain (green), Cx43 (red), and DAPI (blue). *Right*: rotated view of 3D reconstruction through the center of the cell-to-cell junction. *A*: cell pair with a length-to-width ratio (PLW) of 3.5. The height of the junction is 5.9  $\mu\text{m}$ . *B*: cell pair with a PLW of 5.2. The height of the junction is 4.5  $\mu\text{m}$ . *C*: cell pair with a PLW of 7.1. The height of the junction is 3.6  $\mu\text{m}$ . *D*: junction length increases with increasing PLW. *E*: junction height decreases with increasing PLW. *F*: Cx43 immunosignal increases with increasing PLW from 3.5 to 5.2. *G*: junctional conductance ( $g_j$ ) increases with increasing PLW from 3.5 to 5.2. Values are means  $\pm$  SD. \* $P < 0.05$ , ANOVA.

stacks were collected with 300-nm separation between slices ( $z$ -stacks).  $Z$ -stacks were median filtered and deconvolved using blind deconvolution in Huygens Essential (Scientific Volume Imaging, Hilversum, The Netherlands) and imported into Imaris (Bitplane, Zuerich, Switzerland). For each  $z$ -stack, the same threshold was chosen to separate positive Cx43 staining from background staining. The cell-to-cell junction was determined by referencing the bright-field images. The volume of junctional Cx43 was determined by creating isosurfaces in Imaris from the thresholded  $z$ -stack of the Cx43 immunosignal and outputting the volume of the isosurfaces in micrometers cubed. The Cx43 isosurfaces not located in the cell-to-cell junction were not used for the correlation between the electrophysiological measurements and the immunosignal.

To determine parameters characterizing cell shape, cell pairs were fixed and incubated with wheat germ agglutinin (WGA) conjugated to Alexa Fluor 488 (Invitrogen) for 10 min at room temperature. The actual width and length of each cell pair was measured and averaged. The ratio of the length to the width was defined as "cell pair length-to-width ratio" (PLW). To determine the junction height, WGA  $z$ -stacks were imaged using the same protocol mentioned above for Cx43, reconstructed in ImageJ (NIH, Bethesda, MD) and resliced in the  $y$ -plane to facilitate viewing of the junction from the side. Manual measurements of the height of the junction were taken midway through the junction. The length of the cell-to-cell junction was manually measured in ImageJ using maximum projections of the WGA stain.

**Statistics.** All data are reported as mean values  $\pm$  SD. Data were statistically analyzed using ANOVA for comparison between groups, with  $P < 0.05$  considered significant (MATLAB, MathWorks, Natick, MA). Regression lines with  $R^2$  values were determined using the curve-fitting tool of MATLAB.

## RESULTS

**Interface of cell pairs and Cx43 immunosignal.** After 3–5 days in culture, pairs of cells were most commonly observed on a single island or grown across the engineered border (Fig. 2). Pairs spanning two islands with the cell border anchored at the engineered gap were rare (10%) and, therefore, not used. The pairs were subdivided into three groups, with PLW of  $3.5 \pm 0.2$  ( $n = 9$ , Fig. 2A),  $5.2 \pm 0.2$  ( $n = 12$ , Fig. 2B), and  $7.1 \pm 0.4$  ( $n = 10$ , Fig. 2C). As illustrated in Fig. 2, the length of the cell-to-cell junction increased with increasing PLW. Cell pairs with PLW of 3.5, 5.2, and 7.1 had junction lengths of  $24.9 \pm 2.7 \mu\text{m}$  ( $n = 9$ ),  $35.9 \pm 6.4 \mu\text{m}$  ( $n = 11$ ), and  $48.9 \pm 6.2 \mu\text{m}$  ( $n = 10$ ), respectively (Fig. 2D). Conversely, the height of the junction was inversely related to PLW, with junction heights of  $5.7 \pm 1.2 \mu\text{m}$  ( $n = 9$ ),  $4.5 \pm 1.1 \mu\text{m}$  ( $n = 10$ ), and  $4.0 \pm 0.6 \mu\text{m}$  ( $n = 11$ ) for PLW of 3.5, 5.2, and 7.1, respectively (Fig. 2E). Cx43 immunosignal volumes in the PLW of 3.5, 5.2, and 7.1 groups were  $4.4 \pm 3.1 \mu\text{m}^3$  ( $n = 6$ ),  $15.2 \pm 9.5 \mu\text{m}^3$  ( $n = 7$ ), and  $12.7 \pm 7.1 \mu\text{m}^3$  ( $n = 6$ ), respectively (Fig. 2F). Cell pairs with PLW of 3.5, 5.2, and 7.1 had an average  $g_j$  of  $24.7 \pm 15.9 \text{ nS}$  ( $n = 8$ ),  $66.6 \pm 37.6 \text{ nS}$  ( $n = 11$ ), and  $39.2 \pm 22.7 \text{ nS}$  ( $n = 7$ ), respectively (Fig. 2G). Both the increases of Cx43 immunofluorescence and  $g_j$  between PLW 3.5 and 5.2 were statistically significant ( $P < 0.05$  and  $P < 0.01$ , respectively). Increasing PLW beyond 5.2 did not further increase Cx43 immunofluorescence or  $g_j$  (Fig. 2, F and G).

**Electrical cell-to-cell coupling.** To assess the functional consequences of the mixed Cx43/Cx45 composition of rat ventricular gap junctions, we analyzed single gap junction channel currents, as shown in Fig. 3. Figure 3A illustrates four

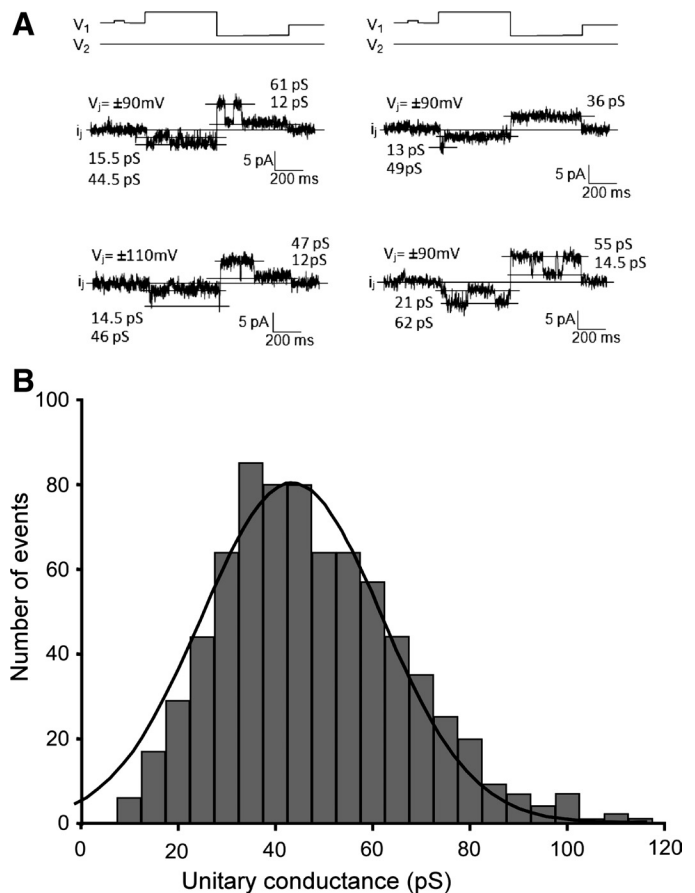


Fig. 3. Dual-voltage clamp in patterned cell pairs and analysis of single gap junction channels. *A*: illustration of four measurements showing openings of single gap junction channels to a full open state and to substates. Note that, depending on polarity of junctional voltage ( $V_j$ ), the channels have a different conductance. This suggests the presence of mixed Cx43/Cx45 channels (see DISCUSSION). *B*: histogram summarizing the measurements of single channels. The Gaussian fit shows a peak at 45 pS ( $\pm 0.8$  pS;  $R^2 = 0.96$ ;  $n = 745$ ).

individual recordings of openings of single gap junction channels. To assess the change in  $\gamma_j$  upon the change in  $V_j$ , recordings were selected that showed only one single-channel opening. In the depicted traces, the difference between  $\gamma_j$  of the last opening before the change in polarity of  $V_j$ , and  $\gamma_j$  of the first opening after the change in  $V_j$ , ranged from 1 to 15 pS (17). For the nine recordings in which one channel opening was observed during the clamp at both polarities of  $V_j$ , the difference in  $\gamma_j$  upon the change in polarity amounted to  $12.9 \pm 2.6$  pS. This was significantly different from the level of noise in each trace ( $P < 0.05$ ), which amounted to  $1.1 \pm 0.1$  pS. As shown in Fig. 3B, the distribution of single-channel conductances yielded a close fit to a Gaussian with a peak at 45 pS ( $\pm 0.8$  pS;  $R^2 = 0.96$ ;  $n = 745$ ). This frequency distribution of  $\gamma_j$  values was closely similar to the distribution in wild-type murine ventricular myocyte pairs (3). The single-channel recordings favor the hypothesis that rat ventricular gap junction channels are composed of mixed heteromeric Cx43-Cx45 connexons (see DISCUSSION).

**Correlation between  $g_j$  and Cx43 immunosignal.** The major goal of this study was to correlate the junctional Cx43 immunosignal to the electrical properties of its cell-to-cell junction. To do this, we patched cell pairs and then fixed and immuno-

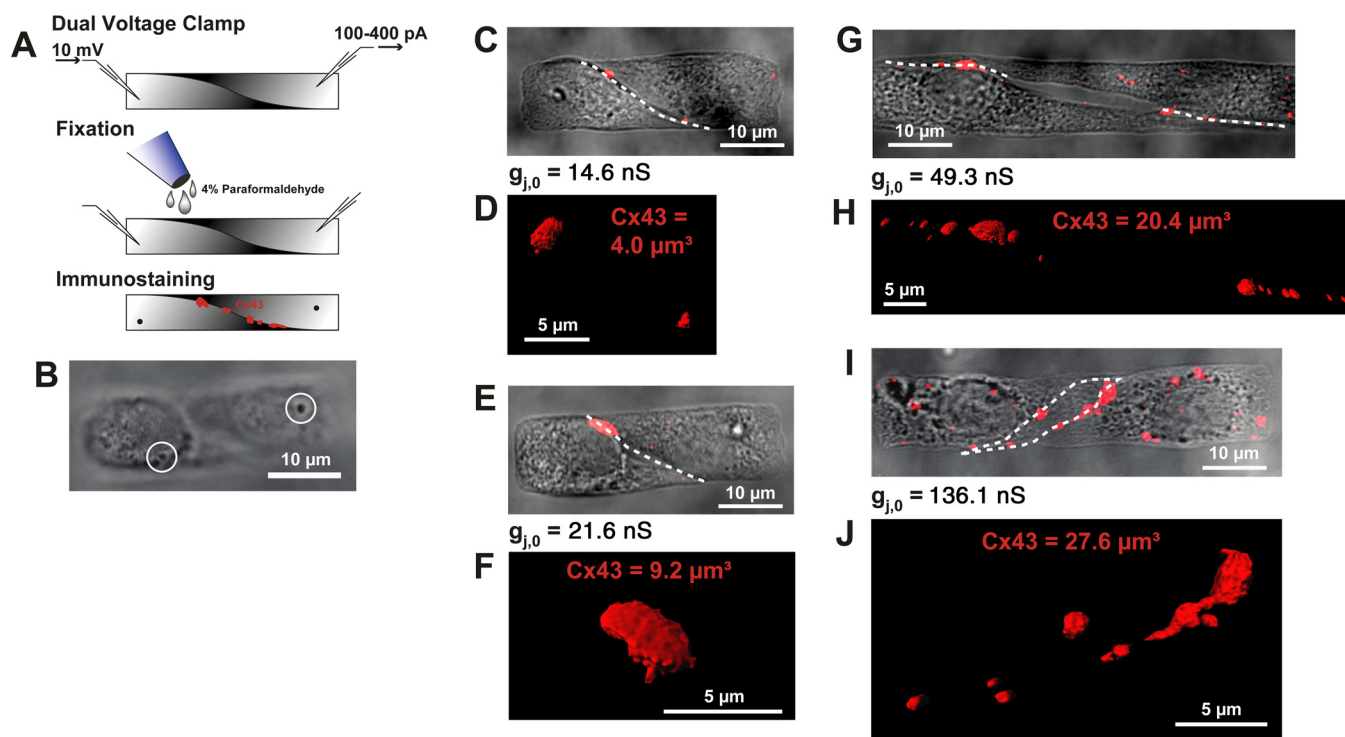


Fig. 4. Relationship between Cx43 immunofluorescence and  $g_j$  in individual cell pairs. **A**: illustration of procedure used to correlate Cx43 immunofluorescence and  $g_j$  in individual pairs. Following dual-voltage clamp recordings, cardiomyocyte pairs were immediately fixed and immunostained for Cx43, which was followed by quantitative image analysis. **B**: the withdrawal of the patch electrodes after fixation enabled the identification of the pair by the suction marks of the electrodes (white circles), in addition to the labeling system shown in Fig. 1. **C–J**: phase-contrast images of representative patched cardiomyocytes pairs (**C**, **E**, **G**, **I**) are overlaid with the contour of the cell-to-cell junction (white dashed lines) and the maximum projection of Cx43 immunofluorescence (red). 3D reconstructions of the junctional Cx43 immunosignal (**D**, **F**, **H**, **J**) are shown. The measured Cx43 volume and  $g_j$  are indicated for each pair.

stained against Cx43 to directly correlate the conductance  $g_j$  with the presence of Cx43 at the cell-cell junction, as illustrated schematically in Fig. 4A. Figure 4B illustrates a cell pair used to correlate  $g_j$  to the Cx43 immunosignal and shows the suction marks of the patch-clamp pipettes in a confocal slice near the top of the z-stack. This suction mark, together with the label of the patterned square (Fig. 1), allowed for the direct correlation between the Cx43 immunosignal and  $g_j$  in each individual pair. This relationship is illustrated for four cell pairs in Fig. 4, **C** and **D**, **E** and **F**, **G** and **H**, and **I** and **J**, ordered according to increasing value of  $g_j$ . The plaque shape of the junctions in the *Y/Z* projection is demonstrated in the 3D animation showing Cx43 immunofluorescence in the pair shown in Fig. 4, **I** and **J** (Supplemental Movie S1; the online version of this article contains supplemental data). Of note, the pair with the largest PLW ratio (Fig. 4, **G** and **H**) had a smaller  $g_j$  and Cx43 immunofluorescence signal than the pair with the smaller PLW ratio shown in Fig. 4, **I** and **J**. This was due to the formation of a cleft in the center of the interface between the pair with the largest PLW (Fig. 4G).

The summarized data of the correlation between the Cx43 immunosignal and  $g_j$  is presented in Fig. 5, in which each point represents a cell pair ( $n = 15$ ). The total Cx43 signal showed a positive correlation to  $g_j$ , with exception of one outlier value (79.8 nS vs.  $10.7 \mu\text{m}^3$ ), which deviated from this correlation. Between 0 and  $25 \mu\text{m}^3$  Cx43 immunosignal, the dependence of  $g_j$  was highly linear ( $R^2 = 0.83$ ). However, the two cell pairs with Cx43 immunosignals  $> 25 \mu\text{m}^3$  showed a very high value of  $g_j$  (exponential fit:  $R^2 = 0.70$ ). This deviation from linearity

may be related to the very large interference of the electrode access resistances at this level of coupling (see DISCUSSION) (31, 34). Interestingly, the correlation line does not pass through the origin. The observation that the “zero intersect” of the correlation corresponds to an average  $g_j$  level of  $\sim 10$  nS (corresponding to  $\sim 100$  channels in the open state) suggests a lower limit for immunofluorescence detection of Cx43 in gap junctions in our experiments (see DISCUSSION).

## DISCUSSION

As a main finding of this study, our experiments show a linear correlation between the  $g_j$  of patterned cell pairs and the Cx43 immunosignal within a range of electrical conductances of 8–50 nS in rat ventricular cardiomyocytes. Moreover, the measurements of single-channel conductances suggest the presence of mixed Cx43/Cx45 channels in the engineered neonatal ventricular rat myocytes.

Soft lithography and microcontact printing techniques were used to control the dimensions of cell pairs used for DVC experiments. Because isolated cardiomyocytes generally conserve their volume (15), we were able to increase the height of the cells by decreasing the surface area of the pattern. The ability to modulate cell height was especially advantageous for DVC experiments because increased cell height reduces the amount of strain on the cell membrane during seal formation with the pipette, thereby minimizing damage to the cell. Micropatterning also increased the probability of cell pair formation, compared with plating cells seeded at random onto an

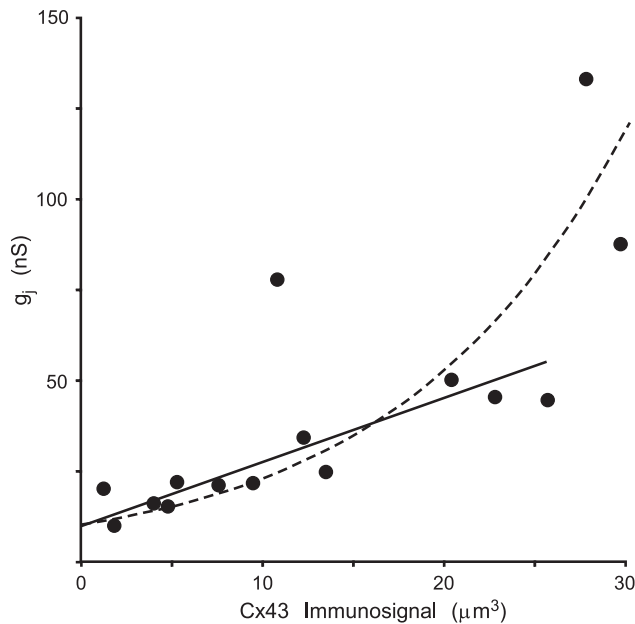


Fig. 5. Relationship between Cx43 fluorescence and  $g_j$  in individual cell pairs. Each point on the graph illustrates the relationship between  $g_j$  and the Cx43 immunosignal in an individual pair for a total of 15 cell pairs. With exception of one outlier value, there is direct relationship between the two parameters. Between 0- and 25- $\mu\text{m}^3$  Cx43 immunosignal, the dependence of  $g_j$  is highly linear ( $R^2 = 0.83$ ). However, the two cell pairs with Cx43 immunosignals  $> 25 \mu\text{m}^3$  showed a very high value of  $g_j$  (exponential fit to the whole data set showed an  $R^2 = 0.70$ ; see DISCUSSION).

isotropic surface. Another advantage of micropatterning is the ability to reproduce cell shape and, therefore, investigate how cell shape contributes to cell-to-cell electrical coupling. Because of the constraints imposed by the pattern, the cell pairs formed cell-to-cell interfaces with consistent junction lengths and heights for a given PLW, demonstrating the ability of microcontact printing to regulate both cell shape and properties of the cell-to-cell interface. For our experiments, there were consistent increases in junction length and decreases in junction height as PLW increased. The  $g_j$  and Cx43 immunofluorescence showed a significant increase with increasing PLW from 3.5 to 5.2, suggesting that gap junction formation was related to junction length. However, increasing PLW further to 7.1 did not show further increases of either  $g_j$  or Cx43 immunosignal. This was most likely due to 1) the decrease in cell height (Fig. 1); and 2) frequent formation of gaps in the center of the cell pair interface at high PLW (Fig. 4, *G* and *H*).

A goal of this study was to correlate the immunofluorescence signals of junctional Cx43 to the intercellular electrical conductance  $g_j$ . It has been shown previously that reduction of Cx43 expression is associated with a decrease in average cumulated gap junction length and number of gap junctions, whereas the average size and size distribution of gap junctions remain the same (24). Our finding of a linear relationship between the Cx43 immunosignal and  $g_j$  within a given range of junctional conductances from  $\sim 8$  to 50 nS supports the notion that the Cx43 immunosignal is a measure of integrated gap junction size or area at the cell interface rather than gap junction protein. Moreover, the present work suggests that there is a lower threshold for immunodetection of gap junction size, below which significant electrical coupling can still be

detected. In our work, the electrical conductance corresponding to this threshold amounted to  $\sim 8$  nS (intersect of linear and exponential fits with ordinate in Fig. 5*B*). Theoretical computations of the relationship between electrical propagation velocity and cell-to-cell resistance have shown that, independent of the model (continuous vs. discontinuous), propagation velocity in linear structures is relatively insensitive to changes in the level of cell-to-cell coupling (25). These arguments together suggest that electrical ventricular propagation, albeit at a significantly lower level, can be preserved in the absence of detectable immunosignal for Cx43. The suggestion that very low levels of Cx43 are not detectable by immunofluorescence is also supported from the comparison of  $g_j$  measurements in cultured rat (our study) and murine cell pairs (3) with genetic ablation of Cx43. Full Cx43 knock out in murine cell pairs produced a decrease of average  $g_j$  to 1.4 nS (3), i.e., to a level amounting to  $\sim 15\%$  of the  $g_j$  level at the Cx43 immunodetection threshold. The observation of an immunodetection threshold of cell-to-cell coupling may, at least partially, explain several previously obtained observations in experimental and pathological settings. In a mouse model of conditional knock-out of Cx43, which increased with age, ventricular arrhythmias and inducible ventricular tachycardias started to occur only at markedly reduced levels of Cx43 immunosignals in gap junctions (7). In arrhythmogenic right ventricular cardiomyopathy in humans, a condition most frequently associated with desmosomal mutations, Cx43 in gap junctions is downregulated and shows a faint immunosignal. Although arrhythmogenic right ventricular cardiomyopathy patients frequently die from ventricular tachycardia, their hemodynamic function before the arrhythmic event is not markedly impaired, which implicates significant cell-to-cell communication in the working myocardium, despite postmortem evidence of markedly reduced Cx43 in right and left ventricular myocardium (2).

The determination of  $g_j$  at high levels of cell-to-cell coupling is hampered by the fact that the sum of the access resistances of the patch electrodes largely determines the flow of current in the measuring circuit. A small change of these values during the experiment may, therefore, introduce an error in the measurements of  $g_j$  (31, 34). The correlation between Cx43 immunofluorescence signals and  $g_j$  at high levels of coupling has, therefore, to be interpreted with caution.

Immunofluorescence signals for Cx45 have been shown to be present in small amounts in rat, mouse, and human ventricles (3, 18, 33, 35). The low level of Cx45 in ventricular myocardium was confirmed in our study, and interference from background fluorescence precluded a quantitative 3D analysis of this immunosignal. Despite its small quantitative contribution, Cx45 may play a modulatory role in ventricular cell-to-cell coupling. Cx45 has been implicated in electrical remodeling in left ventricular hypertrophy and may play a role in limiting gap junction size (16, 35). Moreover, knock out of the coxsackie-adenovirus receptor protein both specifically decreases Cx45 expression in gap junctions and concomitantly increases intercellular dye diffusion between ventricular myocytes (21). In our study, two observations indicate a functional role for Cx45 in rat ventricle. First, the frequency distribution of  $\gamma_j$  showed a peak at 45 pS for the main channel states. These data, which are almost superimposable to the findings in wild-type murine ventricular cells pairs (3), indicate that Cx45 may decrease average  $\gamma_j$ , compared with a population of pure,

homomeric-homotypic Cx43 channels (23, 30). Second, we observed a significant change of gap junction channel conductance upon a switch in the polarity of  $V_j$ . This suggests the presence of channels composed of different heteromeric Cx45/Cx43 mixtures. Since the presence of consecutive single-channel openings, as shown in Fig. 3A, during a voltage clamp does not assert that the openings can be attributed to the same channel, these measurements are not fully conclusive. However, the immunofluorescence data in this and earlier studies, the single-channel measurements, and the earlier observations of heteromeric Cx43/Cx45 formation in heterologous expression systems make it highly likely that Cx43 and Cx45 form heteromeric connexons and mixed gap junction channels in rat ventricle (6, 11).

A potential limitation of our study may be due to the fact that we assessed cell junctions that have been reformed from association of dissociated cells. However, none of the multiple studies involving neofunction of cell junctions in cultured cardiac or heterologous cell systems has shown basic differences in gap junction composition compared with gap junctions in vivo.

In summary, our study demonstrates a direct correlation between the volume occupied by the Cx43 immunosignal and intercellular electrical conductance. Although we did not associate levels of electrical coupling  $<7$  nS with immunofluorescence, this observation raises the question of whether immunofluorescence can detect very small, but still electrically conducting, gap junctions.

#### GRANTS

This work was supported by the Nanoscale Science and Engineering Center of the National Science Foundation (NSF) and the Harvard Materials Research Science and Engineering Center. This study was also supported by the Swiss NSF (A. G. Keber), the Roche Foundation (M. L. McCain), American Heart Association (M. L. McCain), National Heart, Lung, and Blood Institute RO1 HL079126 (K. K. Parker), and NSF OMR-0213805 (Harvard Materials Research and Engineering Center).

#### DISCLOSURES

No conflicts of interest, financial or otherwise, are declared by the author(s).

#### AUTHOR CONTRIBUTIONS

Author contributions: M.L.M., T.D., H.O., and A.G.K. performed experiments; M.L.M., T.D., B.R.-R., and A.G.K. analyzed data; M.L.M., T.D., K.K.P., and A.G.K. interpreted results of experiments; M.L.M., T.D., and A.G.K. prepared figures; M.L.M., K.K.P., and A.G.K. drafted manuscript; M.L.M., T.D., N.A.G., B.R.-R., K.K.P., and A.G.K. edited and revised manuscript; M.L.M., T.D., N.A.G., B.R.-R., K.K.P., and A.G.K. approved final version of manuscript; T.D., N.A.G., B.R.-R., K.K.P., and A.G.K. conception and design of research.

#### REFERENCES

- Ai X, Pogwizd SM. Connexin 43 downregulation and dephosphorylation in nonischemic heart failure is associated with enhanced colocalized protein phosphatase type 2A. *Circ Res* 96: 54–63, 2005.
- Asimaki A, Tandri H, Huang H, Halushka MK, Gautam S, Basso C, Thiene G, Tsatsopoulou A, Protonotarios N, McKenna WJ, Calkins H, Saffitz JE. A new diagnostic test for arrhythmogenic right ventricular cardiomyopathy. *N Engl J Med* 360: 1075–1084, 2009.
- Beauchamp P, Choby C, Desplantez T, de Peyer K, Green K, Yamada KA, Weingart R, Saffitz JE, Kleber AG. Electrical propagation in synthetic ventricular myocyte strands from germline connexin43 knockout mice. *Circ Res* 95: 170–178, 2004.
- Beauchamp P, Yamada KA, Baertschi AJ, Green K, Kanter EM, Saffitz JE, Kleber AG. Relative contributions of connexins 40 and 43 to atrial impulse propagation in synthetic strands of neonatal and fetal murine cardiomyocytes. *Circ Res* 99: 1216–1224, 2006.
- Bray MA, Sheehy SP, Parker KK. Sarcomere alignment is regulated by myocyte shape. *Cell Motil Cytoskeleton* 65: 641–651, 2008.
- Cottrell GT, Burt JM. Functional consequences of heterogeneous gap junction channel formation and its influence in health and disease. *Biochim Biophys Acta* 1711: 126–141, 2005.
- Danik SB, Liu F, Zhang J, Suk HJ, Morley GE, Fishman GI, Gutstein DE. Modulation of cardiac gap junction expression and arrhythmic susceptibility. *Circ Res* 95: 1035–1041, 2004.
- Darrow BJ, Fast VG, Kléber AG, Beyer EC, Saffitz JE. Functional and structural assessment of intercellular communication: increased conduction velocity and enhanced connexin expression in dibutyl cAMP-treated cultured cardiac myocytes. *Circ Res* 79: 174–183, 1996.
- Davis LM, Kanter HL, Beyer EC, Saffitz JE. Distinct gap junction protein phenotypes in cardiac tissues with disparate conduction properties. *J Am Coll Cardiol* 24: 1124–1132, 1994.
- Desplantez T, Halliday D, Dupont E, Severs NJ, Weingart R. Influence of v5/6-His tag on the properties of gap junction channels composed of connexin43, connexin40 or connexin45. *J Membr Biol* 240: 139–150, 2011.
- Desplantez T, Halliday D, Dupont E, Weingart R. Cardiac connexins Cx43 and Cx45: formation of diverse gap junction channels with diverse electrical properties. *Pflügers Arch* 448: 363–375, 2004.
- Dupont E, Matsushita T, Kaba RA, Vozzi C, Coppens SR, Khan N, Kaprielian R, Yacoub MH, Severs NJ. Altered connexin expression in human congestive heart failure. *J Mol Cell Cardiol* 33: 359–371, 2001.
- Elenes S, Rubart M, Moreno AP. Junctional communication between isolated pairs of canine atrial cells is mediated by homogeneous and heterogeneous gap junction channels. *J Cardiovasc Electrophysiol* 10: 990–1004, 1999.
- Fedorov VV, Lozinsky IT, Sosunov EA, Anyukhovskiy EP, Rosen MR, Balke CW, Efimov IR. Application of blebbistatin as an excitation-contraction uncoupler for electrophysiologic study of rat and rabbit hearts. *Heart Rhythm* 4: 619–626, 2007.
- Geisse NA, Sheehy SP, Parker KK. Control of myocyte remodeling in vitro with engineered substrates. *In Vitro Cell Dev Biol Anim* 45: 343–350, 2009.
- Grikscheit K, Thomas N, Bruce AF, Rothery S, Chan J, Severs NJ, Dupont E. Coexpression of connexin 45 with connexin 43 decreases gap junction size. *Cell Commun Adhes* 15: 185–193, 2008.
- Harris AL. Emerging issues of connexin channels: biophysics fills the gap. *Q Rev Biophys* 34: 325–472, 2001.
- Johnson CM, Kanter EM, Green KG, Laing JG, Betsuyaku T, Beyer EC, Steinberg TH, Saffitz JE, Yamada KA. Redistribution of connexin45 in gap junctions of connexin43-deficient hearts. *Cardiovasc Res* 53: 921–935, 2002.
- Kanter H, Saffitz J, Beyer E. Cardiac myocytes express multiple gap junction proteins. *Circ Res* 70: 438–444, 1992.
- Kleber AG, Rudy Y. Basic mechanisms of cardiac impulse propagation and associated arrhythmias. *Physiol Rev* 84: 431–488, 2004.
- Lisewski U, Shi Y, Wrackmeyer U, Fischer R, Chen C, Schirdewan A, Jüttner R, Rathjen F, Poller W, Radke MH, Gotthardt M. The tight junction protein CAR regulates cardiac conduction and cell-cell communication. *J Exp Med* 205: 2369–2379, 2008.
- Rohr S, Schölly DM, Kléber AG. Patterned growth of neonatal rat heart cells in culture: Morphological and electrophysiological characterization. *Circ Res* 68: 114–130, 1991.
- Saez JC, Moreno AP, Spray DC. Norepinephrine induces  $Ca^{2+}$  release from intracellular stores in rat pinealocytes. *J Pineal Res* 16: 57–64, 1994.
- Saffitz JE, Green KG, Kraft WJ, Schechtman KB, Yamada KA. Effects of diminished expression of connexin43 on gap junction number and size in ventricular myocardium. *Am J Physiol Heart Circ Physiol* 278: H1662–H1670, 2000.
- Shaw RM, Rudy Y. Ionic mechanisms of propagation in cardiac tissue. Roles of the sodium and L-type calcium currents during reduced excitability and decreased gap junction coupling. *Circ Res* 81: 727–741, 1997.
- Singhvi R, Kumar A, Lopez GP, Stephanopoulos GN, Wang DI, Whitesides GM, Ingber DE. Engineering cell shape and function. *Science* 264: 696–698, 1994.
- Thomas SP, Bircher-Lehmann L, Thomas SA, Zhuang J, Saffitz JE, Kleber AG. Synthetic strands of neonatal mouse cardiac myocytes: structural and electrophysiological properties. *Circ Res* 87: 467–473, 2000.

28. **Thomas SP, Kucera JP, Bircher-Lehmann L, Rudy Y, Saffitz JE, Kleber AG.** Impulse propagation in synthetic strands of neonatal cardiac myocytes with genetically reduced levels of connexin43. *Circ Res* 92: 1209–1216, 2003.
29. **Valiunas V, Bukauskas FF, Weingart R.** Conductances and selective permeability of connexin43 gap junction channels examined in neonatal rat heart cells. *Circ Res* 80: 708–719, 1997.
30. **Valiunas V, Bukauskas FF, Weingart R.** Conductances and selective permeability of connexin43 gap junction channels examined in neonatal rat heart cells. *Circ Res* 80: 708–719, 1997.
31. **Van Rijen HV, Wilders R, Van Ginneken AC, Jongsma HJ.** Quantitative analysis of dual whole-cell voltage-clamp determination of gap junctional conductance. *Pflügers Arch* 436: 141–151, 1998.
32. **van Veen AA, van Rijen HV, Opthof T.** Cardiac gap junction channels: modulation of expression and channel properties. *Cardiovasc Res* 51: 217–229, 2001.
33. **Vozzi C, Dupont E, Coppin SR, Yeh HI, Severs NJ.** Chamber-related differences in connexin expression in the human heart. *J Mol Cell Cardiol* 31: 991–1003, 1999.
34. **Wilders R, Jongsma HJ.** Limitations of the dual voltage clamp method in assaying conductance and kinetics of gap junction channels. *Biophys J* 63: 942–953, 1992.
35. **Yamada KA, Rogers JG, Sundset R, Steinberg TH, Saffitz JE.** Up-regulation of connexin45 in heart failure. *J Cardiovasc Electrophysiol* 14: 1205–1212, 2003.

